International Journal on Magnetic Particle Imaging
Vol 9, No 1, Suppl 1, Article ID 2303060, 5 Pages

Infinite Science Publishing

Proceedings Article

Simulation study of a magnetic particle imaging device capable of hyperthermia

Jie He[a] · Yimeng Li[a] · Tao Zhu[b] · Jing Zhong[c] · Hui Hui[b,d,e] · Jie Tian[d,e,f,g,*]

[a]School of Biological Science and Medical Engineering, Beihang University, Beijing, China
[a]University of Chinese Academy of Sciences, Beijing, 100080, China
[a]School of Instrumentantion and Optoelectronic Engineering, Beihang University, Beijing, China
[a]CAS Key Laboratory of Molecular Imaging, Institute of Automation, Beijing, 100190, China
[a]Beijing Key Laboratory of Molecular Imaging, Beijing, 100190, China
[a]Key Laboratory of Big Data-Based Precision Medicine (Beihang University), Ministry of Industry and Information Technology of the People's Republic of China, Beijing, 100191, People's Republic of China
[a]Zhuhai Precision Medical Center, Zhuhai People's Hospital, affiliated with Jinan University, Zhuhai, 519000, China
*Corresponding author, email: jie.tian@ia.ac.cn

Abstract

Magnetic fluid hyperthermia (MFH) is a promising non-invasive therapy. Magnetic particle imaging (MPI) is a novel quantitative imaging technique determining the local concentration of magnetic nanoparticles with high sensitivity, and high temporal-spatial resolution. Successful implemention of MPI-guided localized MFH have been reported, which shows great potential for precision diagnosis and treatment of tumors. However, real-time 3D MPI-guided localized MFH hasn't been reported, which is promising for understaning the the treatment process and molecular mechanism of MFH. Here, we present a proof-of-concept design of a 3D Cartesian scanning MPI device with a radiofrequency coil capable of localized MFH. A proof-of-concept simulation study is conducted to evaluate the feasibility of designed coils, designed 3D MPI mode and designed localized mode. The simultion results show the designed MPI device has the potential to realize the real-time 3D MPI-guided localized MFH.

I. Introduction

Magnetic fluid hyperthermia (MFH) is a promising non-invasive therapeutic approach, which has shown the potential to reduce the adverse side effects of several tumors such as prostate, glioblastoma, and metastatic bone cancer[1] Magnetic particle imaging (MPI) is a novel molecular and cellular imaging modality technique, which uses the nonlinear re-magnetization behavior of magnetic nanoparticles to determine their local concentration[2], [3]. Also, ultilizing the temperature-dependence of MPI spectral signals, simultaneous imaging and temperature mapping has been implemented using a multi-contrast reconstruction approach based on the system matrix[4].

The combination of MPI and MFH (MPI-MFH) has drawn enormous attention and shown great potential for precision diagnosis and treatment of tumors[5-7]. The real-time 3D MPI-guided localized MFH is promising for understaning the the treatment process and molecular mechanism of MFH. However, the real-time 3D MPI-guided localized MFH has not been reported due to the great challenges faced by the fusion of MPI device and MFH device. Here, we present a proof-of-concept of a 3D Cartesian scanning MPI device with an radiofrequency coil, the simultion results show it is promising to realize real-time 3D MPI-guided localized MFH.

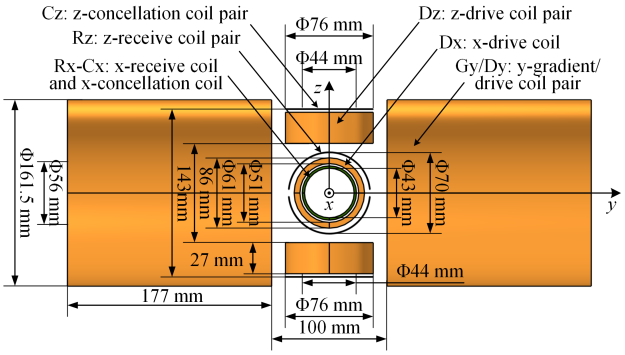

Figure 1: The structure of designed MPI device.

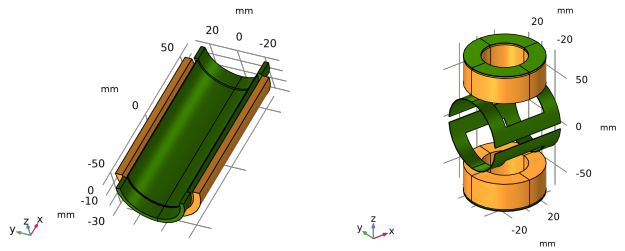

(a) (b)

Figure 2: The 3D structure of (a) the x-receive and concellation coils in a half-section view (in green color) and (b) the z-receive and concellation coils (in green color).

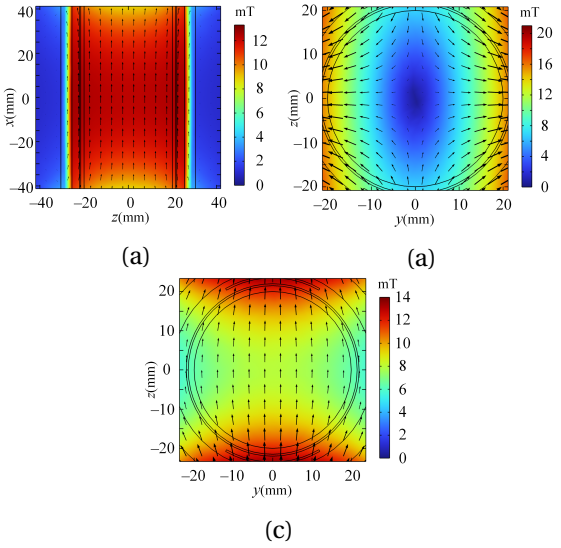

(a) (a)

(c)

Figure 3: MFD of the drive coils. (a) |B| on the ZOX plane from the x-drive coil; (b) |B| on the YOZ plane from the y-gradient/drive coil pair; (c) |B| on the YOZ plane from the z-drive coil pair.

II. Material and methods

II.I. Drive coils

The designed MPI device includes three dimensional drive coils, as shown in Figure 1. The drive coils all use hollow copper wire with 0.5 mm of wall thickness for the excellent thermal contact with the water coolant. The x-drive coil is a 100-mm-long solenoid consisting of 16 windings, which can be used to generate a 300 kHz radiofrequency magnetic field. The y-drive coil pair is used to generate a gradient field and a 10 Hz low-frequency drive field. The y-drive coil pair is wound in the same direction. Each half of the y-drive coil pair is independently powered by one power amplifier. The gradient field is generated when the two halves of the y-drive coil pair are carrying the direct currents with the same amplitude and reverse phase. Meanwhile, the low-frequency drive field is generated when the two halves of the y-drive coil pair are carrying the alternate current with the same amplitude and same phase. The z-drive coil pair is a Helmholtz coil pair used to generate a 25 kHz alternate magnetic field.

The simulation results from COMSOL of the magnetic field distribution of the drive coils are shown in Figure 3. The maximum magnetic gradients in the x-, y- and z-axis are about -3.5, 7 and -3.5 T/m. The maximum amplitudes of magnetic flux density (MFD) in the x-, y- and z-axis are about 13, 150 and 8 mT.

The requirements of magnetic gradients from the same y-drive coil pair are different for 3D MPI and localized MFH. If the magnetic gradients are set very high, the size of field of view (FOV) will be very small due to the limited amplitudes of MFD, which is not enough for 3D MPI. If the magnetic gradients are set very low, the resolution of specific absorption rate (SAR) will be very low, which is not good for localized MFH.

In this work, we perform 3D MPI and localized MFH in the time division multiplexing technology. In 3D MPI mode, we let the magnetic gradients in the x-, y- and z-axis be -0.5, 1, and -0.5 T/m and let the MFD amplitudes in the x-, y- and z-axis be 13, 26 and 8 mT for a 3D Cartesian scanning. In localized MFH mode, since a localized heating of magnetic nanoparticles within 2.35 mm in a 7 T/m gradient field has been reported[8], we let the magnetic gradients in the x-, y- and z-axis be -3.5, 7 and -3.5 T/m, and then let the y- and z-drive coil pairs and the animal bed provide the appropriate offset magnetic field and the appropriate mechanical offset, respectively, to set the field-free point (FFP) in the center of hyperthermia site, the radiofrequency coil is used to generate a radiofrequency magnetic field with changeable amplitude to heat the magnetic nanoparticles. In 3D MPI mode and localized MFH mode, the radiofrequency coil keeps the same frequency, thus the transition time between the two modes is short, which makes the real-time 3D MPI-guided localized MFH possible.

10.18416/ijmpi.2023.2303060

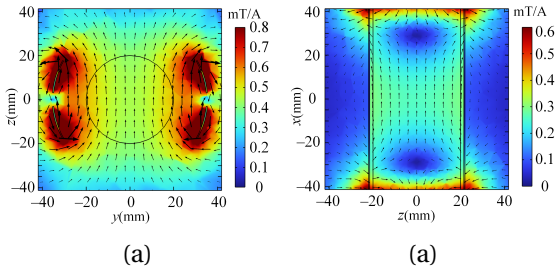

Figure 4: Sensitivity of the receive coils. (a) Sensitivity on the YOZ plane of the z-receive coil pair; (b) Sensitivity on the ZOX plane of the x-receive coil.

II.II. Receive and cancellation coils

The designed MPI device includes receive and cancellation coils in x and z directions, their 3D structures are shown in Figure 2. The receive and cancellation coils all use litz wire for lessening the skin effect of 300 kHz/25 kHz alternating current, the litz wire is submillimeter in diameter, for the sake of simplicity, we only marked the internal diameters of receive and cancellation coils in Figure 1. The x-receive coil is a 100-mm-long and 0.5-mm-thick solenoid consisting of 32 windings, meanwhile, half of the x-cancellation coil pair is a 10-mm-long and 3-mm-thick solenoid consisting 48 windings. Half of the z-receive coil pair is a 0.5-mm-thick long curved rectangle consisting of 24 windings, meanwhile, half of the z-cancellation coil pair is a 0.5-mm-thick ring consiting 30 windings. Based on the above configuration of receive and cancellation coils, the feed-through signals in x and z receive coils are both attenuated by at least 40 dB. Also, we present the simulation results from COMSOL of the sensitivity distribution of the receive coils in Figure 4.

III. Experimental setup

We have presented the magnetic field distribution of the drive coils in Figure 3 and the sensitivity distribution of the receive and cancellation coils in Figure 4, we further list the electrical parameters of these coils in Table 1. Based on these results, we would say that the coil design of our designed MPI device is basically feasible.

In order to illustrate the feasibility of multi-contrast reconstruction approach based on the system matrix[4] with our proposed 3D Cartesian trajectory, we performed a simple simulation using MATLAB. We take the Debye model[9] to characterize the magnetization response of magnetic nanoparticles. The parameters of magnetic nanoparticles are set according to Perimag-COOH®, the parameters are as follows: magnetic core of 130 nm[10], saturation magnetization of about 100 A/m[11], constant tau values of 1.7 µs at 25 ℃ and 2.0 µs at 35 ℃[12]. Also, we add a -40 dB Guassian noise to the simulated system matrix with a undiluted (5 mg/mL) sample point,

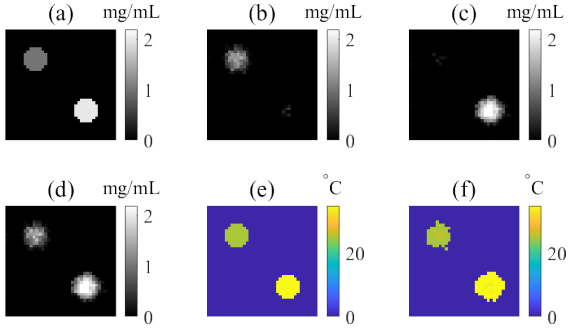

Figure 5: The results of multi-contrast reconstruction approach based on the system matrix. (a) the concentration map of phantom with two samples at 25 ℃, 1 mg/mL and 35 ℃, 2 mg/mL; (b) the component of reconstructed concentration map in 25 ℃ channel; (c) the component of reconstructed concentration map in 35 ℃ channel; (d) the reconstructed concentration map of 25 ℃ and 35 ℃ channel fused together; (e) the temperature map of phantom with two samples at 25 ℃, 1 mg/mL and 35 ℃, 2 mg/mL; (f) the reconstructed temperature map, a threshold value of 10% of max reconstructed concentration value in (d) is set to reduce noise, only the temperature of the pixels with the concentration value greater than the threshold are mapped.

the frequency components based on the intermodulation theory[13] with a signal to noise ratio (SNR) of 3 are selected. The FOV of 20 mm × 20 mm in XOY plane is discretized at 37 × 37 sampling points. Note that, a 2D FOV instead of 3D FOV is choosed just for the sake of visualization. We take the regularized Kaczmarz algorithm to obtain the solution[14]. The regularization parameter and iterations are set as 10^{-4} and 10,000, respectively.

In order to illustrate the feasibility of our designed localized MFH mode, we further use the above Debye model of Perimag-COOH at 35 ℃ to simulate the spatial localization of heating, as is shown in Figure 6.

Table 1: Electrical parameters of coils of the designed MPI device.

Parameter	Number of turns	Resistance	Inductance	Power
Dx	16	75.00 mΩ	5.10 µH @ 300 kHz	183.71 W @ AC 70 A, 13 mT
Dy	285×2	0.12 Ω	5.48 mH @ 10 Hz	309.86 W @ DC 50 A, 7 T/m; 102.28 W @ AC 40 A, 26 mT
Dz	22×2	35.97 mΩ	45.70 µH @ 25 kHz	115.09 W @ AC 80 A
Rx-Cx*	32+ 48×2	0.79 Ω	188.73 µH @ 300 kHz	/
Rz-Cz*	24×2+ 30×2	2.23 Ω	562.68 µH @ 25 kHz	/

* Rx-Cx (Rz-Cz) denotes the series of Rx and Cx (Rz and Cz).

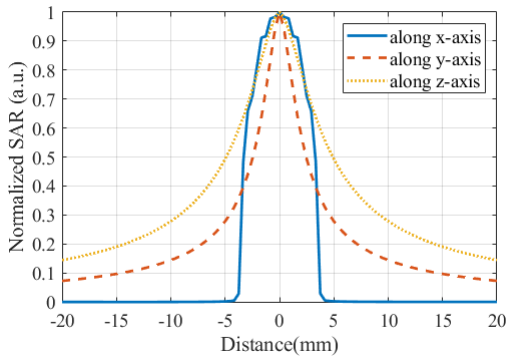

Figure 6: Spatial localization of heating with the Debye model of Perimag-COOH in 1D: simulated SAR vs. distance along the x-, y- and z-axis, the SAR resolutions (the full width at the half maximum of SAR curves) along the x-, y- and z-axis are 6.59 mm, 4.91 mm, and 9.81 mm, respectively.

IV. Results

The phantom consists of one sample of 1 mg/mL at 25 ℃, and the other one of 2 mg/mL at 35 ℃, as is shown in Figure 5 (a) and (e). The mean values of reconstructed concentrations of the two samples in 25 ℃ channel shown in Figure 5 (b) are 0.888 mg/mL and 0.043 mg/mL, respectively, and those in 35 ℃ channel shown in Figure 5 (c) are 0.027 mg/mL and 1.670 mg/mL, respectively. The superposition of the above two concentration map result in Figure 5 (d). The relative error of estimated mean concentrations of the two samples are 1−(0.888+0.027)/1 = 8.50% and 1−(0.043+1.670)/2 = 14.35%. The energy leakage of concentrations is owing to the blurring effect of the regularization parameter in regularized Kaczmarz algorithm, an algorithm with better anti-noise performance may reduce the relative error of estimated mean concentrations. Moreover, based on the linear approximation method in a sufficiently narrow temperature range[4], the estimated mean temperature of the two samples are 25+(35−25)×0.027/(0.027+0.888)=25.295 ℃ and 25+(35−25)×1.670/(0.043+1.670)=34.749 ℃. The absolute error between the estimated mean temperature and real temperatures are 25.295−25=0.295 ℃ and 35−34.749=0.251 ℃, which is acceptable for temperature monitoring in MFH. This means that simultaneous concentration mapping and temperature mapping is basically feasible using our designed MPI device.

Figure 6 shows the spatial localization of heating along the x-, y- and z-axis. The SAR resolutions along the x-, y- and z-axis are 6.59 mm, 4.91 mm and 9.81 mm, respectively. The subcentimeter SAR resolutions provide us the possibility of localized MFH to treat tumors without damaging normal tissues. Besides, the magnetic field gradient in the y direction is twice as that in the x and z direction, and the radiofrequency field in localized MFH mode is along the x direction. This explains the SAR resolutions in order from best to worst are along y-, x- and z-axis.

V. Conclusion

We described the designed MPI device for real-time 3D MPI-guided localized MFH. The designed MPI device could switch quickly between the 3D MPI mode and localized MFH mode by simply changing the drive currents. Several simulations were conducted with COMSOL to illustrate the feasibilty of the coils of our designed MPI device. Moreover, we conducted simulations with MATLAB to illustrate the feasibility of our designed 3D MPI mode and localized MFH mode, the simulation results showed that our designed MPI mode has the potential to realize simultaneous concentration mapping and temperature mapping, and our designed localized MFH mode has the potential to realize subcentimeter SAR resolution. Despite the above simulation results, there are still many factors that need to be considered in the process of design and manufacture: circuit, electromagnetic shielding, mechanical structure, heat management, etc. Given all this, we would say that our designed MPI device capable of hyperthermia is bascially feasible. Our future work will focus on the assembly and adjustment of the designed MPI device.

Acknowledgments

This work was supported in part by the National Key Research and Development Program of China under Grant 2017YFA0700401; the National Natural Science Foundation of China under Grant 62027901, 81827808, 81671851, 81227901; the CAS Youth Innovation Promotion Association under Grant 2018167 and CAS Key Technology Talent Program; the Guangdong Key Research and Development Program of China (2021B0101420005); the Project of High-Level Talents Team Introduction in Zhuhai City (Zhuhai HLHPTP201703). The authors would like to acknowledge the instrumental and technical support of Multimodal Biomedical Imaging Experimental Platform, Institute of Automation, Chinese Academy of Sciences.

Author's statement

Authors state no conflict of interest. Informed consent has been obtained from all individuals included in this study. Conflict of interest: Authors state no conflict of interest. Informed consent: Not applicable. Ethical approval: Not applicable.

References

[1] K. Mahmoudi, A. Bouras, D. Bozec, R. Ivkov, and C. Hadjipanayis, "Magnetic hyperthermia therapy for the treatment of glioblastoma: a review of the therapy's history, efficacy and application in humans," International Journal of Hyperthermia, vol. 34, no. 8, pp. 1316–1328, 2018.

[2] T. Knopp and T. M. Buzug, Magnetic Particle Imaging: An Introduction to Imaging Principles and Scanner Instrumentation. Berlin/Heidelberg: Springer, 2012.

[3] B. Gleich and J. Weizenecker, "Tomographic imaging using the nonlinear response of magnetic particles," Nature, vol. 435, no. 7046, pp. 1214–1217, 2005.

[4] C. Stehning, B. Gleich, and J. Rahmer, "Simultaneous magnetic particle imaging (mpi) and temperature mapping using multi-color mpi," International Journal on Magnetic Particle Imaging, vol. 2, no. 2, 2016.

[5] D. Hensley, Z. W. Tay, R. Dhavalikar, B. Zheng, P. Goodwill, C. Rinaldi, and S. Conolly, "Combining magnetic particle imaging and magnetic fluid hyperthermia in a theranostic platform," Physics in Medicine & Biology, vol. 62, no. 9, p. 3483, 2017.

[6] Y. Du, X. Liu, Q. Liang, X.-J. Liang, and J. Tian, "Optimization and design of magnetic ferrite nanoparticles with uniform tumor distribution for highly sensitive mri/mpi performance and improved magnetic hyperthermia therapy," Nano letters, vol. 19, no. 6, pp. 3618–3626, 2019.

[7] J. Wells, S. Twamley, A. Sekar, A. Ludwig, H. Paysen, O. Kosch, and F. Wiekhorst, "Lissajous scanning magnetic particle imaging as a multifunctional platform for magnetic hyperthermia therapy," Nanoscale, vol. 12, no. 35, pp. 18 342–18 355, 2020.

[8] Z. W. Tay, P. Chandrasekharan, A. Chiu-Lam, D. W. Hensley, R. Dhavalikar, X. Y. Zhou, E. Y. Yu, P. W. Goodwill, B. Zheng, C. Rinaldi et al., "Magnetic particle imaging-guided heating in vivo using gradient fields for arbitrary localization of magnetic hyperthermia therapy," ACS nano, vol. 12, no. 4, pp. 3699–3713, 2018.

[9] L. R. Croft, P. W. Goodwill, and S. M. Conolly, "Relaxation in x-space magnetic particle imaging," IEEE transactions on medical imaging, vol. 31, no. 12, pp. 2335–2342, 2012.

[10] M. Irfan, N. Dogan, T. Sapmaz, and A. Bingolbali, "Development of MPI relaxometer for characterization of superparamagnetic nanoparticles." Journal of Magnetism and Magnetic Materials, vol. 536, pp. 168082, 2021.

[11] T. J. Carter, "Magnetic hyperthermia for the treatment of glioblastoma," Diss. UCL (University College London), 2019.

[12] M. Utkur and E. Ü. Sarıtaş, "Temperature mapping via relaxation-based color MPI", International Journal on Magnetic Particle Imaging, vol. 6, no. 2 Suppl 1, 2020.

[13] K. Button, "Microwave ferrite devices: The first ten years," IEEE Transactions on Microwave Theory and Techniques, vol. 32, no. 9, pp. 1088–1096, 1984.

[14] T. Knopp, J. Rahmer, T. F. Sattel, S. Biederer, J. Weizenecker, B. Gleich, J. Borgert, and T. M. Buzug, "Weighted iterative reconstruction for magnetic particle imaging," Physics in medicine & biology, vol. 55, no. 6, p. 1577, 2010.

10.18416/ijmpi.2023.2303060